Springer

KSME

Journal of Mechanical Science and Technology 30 (11) (2016) 4845~4857
www.springerlink.com/content/1738-494x(Print)/1976-3824(Online)
DOI 10.1007/s12206-016-1003-y

Study on stress states of a wheelset axle due to a defective wheel †

Xingwen Wu* and Maoru Chi

State Key Laboratory of Traction Power, Southwest Jiaotong University, Chengdu, China

(Manuscript Received November 27, 2015; Revised March 22, 2016; Accepted June 18, 2016)

Abstract

High magnitude impact loads caused by a defective wheel may excite various vibration modes of the wheelset, and contribute to adversely increases in the stress states of wheelset axle in high-speed conditions. In this study, the wheelset is treated as a flexible body using the finite element method, then integrated to a multi-body dynamic model of a high-speed train coupled with a flexible track slab model. Through this model the effects of wheel defects considering wheel flats and wheel polygonalizations on the stress states of wheelset axle are evaluated in terms of bending stresses of the wheelset axle. The damage tolerances of the wheelset axle are subsequently predicted using the NASGRO algorithm. The results suggest that the impact forces caused by wheel flats and wheel polygonalizations at the wheel-rail interfaces can result in the resonance vibrations of a wheelset and give rise to severe variations in dynamic stresses of the wheelset axle. The wheel defects-induced stress load cycles considerably contribute to the propagations of the initial crack in the wheelset axle, especially for the wheel polygonalization.

Keywords: Wheel flat; Wheel polygonalization; Flexible wheelset; Slab track; Dynamic stress of wheelset axle; High speed train; NASGRO; Damage tolerance analysis

1. Introduction

The wheels of railway vehicles invariably exhibit some imperfections attributed to either the manufacturing defects or wear caused by wheel/rail interactions. The imperfections on the wheels, usually referred to as wheel defects, can impose considerable impact loads at the wheel/rail interface leading to severe damages to the vehicle-track system including the wheelsets, bearings, rails, sleepers and the track foundation [1]. In addition, it also substantially increases the maintenance costs associated with re-profiling of the wheels. In North America the railway industry spends nearly $90 million annually to replace 125000 wheels due to the wheel defects, while the spalled wheels alone cost $15 million annually [2].

Wheel defects primarily include flats, shelling, spalling, wheel corrugation and wheel polygonalization. The flats, shelling and spalling are usually regarded as local defects with shorter wavelength, while the wheel corrugations and polygonalization are defects with longer wavelength around the wheel circumference [1]. The occurrences of these defects can generate high magnitudes of impact forces between wheel/rail interfaces in high-speed trains. According to the existing investigations, two types of wheel defects, namely, wheel flats and wheel polygonalizatons, are frequently observed in high-speed trains. Thus, the main objectives of this study mainly focus on wheel flats and wheel polygonalizations.

A wheel flat is a flat spot on the rolling surface of a wheel generally caused by sliding of the wheel on the rail. The wheel sliding could be attributed to poorly adjusted, frozen or defective brakes, or high level of braking forces compared with the available wheel/rail adhesion. The contaminations on the rail, including leaves, grease, frost and snow, are also regarded as another critical contributor of the wheel flat [3]. The geometry of a wheel flat is commonly described by either a chord-flat or a cosine-flat [4]. A chord-type flat represents a newly formed wheel flat with sharper edges. During service, such sharper edges of chord-type flat tend to become more rounded, which is more adequately described by a cosine-type flat, also referred to as a haversine flat. The effects of flats on wheel/rail impacts considering a haversine flat have been widely investigated theoretically and experimentlly [5-11]. Through a finite element model of the vehicle-track system, Dukkipati and Dong [10] concluded that the magnitudes of impact loads due to wheel flats are strongly affected by the shape and size of the flat, axle load, vehicle speed and rail-pad stiffness, and reducing the rail-pad stiffness could lower the magnitude of impact forces. Johansson and Nielsen [12] investigated the wheel flats-induced impact forces experimentally and analytically. The study presented validations of two types of track models, namely, the linear [13] and the state-dependent [6] track model using the measured data. The results suggested that the

*Corresponding author. Tel.: +86 13678081221, Fax.: +86 28 86466221
E-mail address: xingwen_wu@163.com
† Recommended by Associate Editor Byeng Dong Youn

linear model underestimates peak wheel/rail impact forces up to the speed of 50 km/h, and overestimates the forces above 70 km/h. Although the state-dependent track model showed better agreements with the measured data, it also overestimated the impact forces for speeds above 70 km/h.

The polygonal wear of railway wheel is a periodic uneven wear on the wheel circumference. In the past decades, the low order polygonal wear such as 1st order and 3rd order, were often observed in wheels of freights and conventional passenger cars [1], while the higher order polygonal wear (20th order) has been observed in high speed trains recently [14]. Such polygonal wear adversely affects the ride comfort of passengers and safety of vehicle components [15]. The mechanism of the polygonal wear, however, has not yet been clearly understood. Using the perturbation techniques and the method of multiple time scales, Brommundat [16] theoretically studied the growth of wheel non-circularity due to wheel/rail interactions and the rotational inertial of wheels. The results suggested that the increase in speed can lead to rapid growth in lower harmonics of the non-circularity.

Morys [17] proposed a long term wear accumulation iteration model together with a coupled vehicle/track dynamic model and a short term wear model to investigate the growth in wheel polygonalization for an ICE (InterCity Express) passenger car. In the model, the wheelset was represented by 8 rigid bodies coupled through three dimensional damped spring elements to consider the bending and torsional elasticity. The long term wear model was based on the hypothesis of short term wear model considering that the mass excavation at each point of the wheel circumference is proportional to the wear energy within the contact patch. The results suggested that the normal force variations due to the wheel polygonalization can excite the bending oscillations of the wheelset axle lending to lateral slips between the wheel and the rail and lateral material excavations. Johansson and Andersson [18] also used similar iterative approach to study the out-of-roundness of wheels and concluded that the wheel polygonalizations are attributed to vertical resonance of vehicle/track system near 40 Hz, and the lowest vertical track anti-resonance near 165 Hz.

A number of studies have been employed to study the effects of wheel polygonalization on dynamic performance of vehicles [14, 15, 19-21]. Using a vertical vehicle/track coupled dynamic model, Liu [21] reported that a polygonal wheel generates considerable fluctuations in the wheel/rail contact forces, and the impact forces become more sensitive with increasing speed, especially for the high order polygonal wheels. Zhang [14] investigated the relationships between the polygonal wear and the noise generation in a high-speed train experimentally and theoretically, and suggested that the polygonal wear strongly affects the noise level emitted by the wheel/rail interactions.

The aforementioned investigations mainly focused on impact forces and noise generations caused by wheel defects at the wheel/rail interfaces, while the stress states of the wheelset axle in the presence of wheel defects have not yet been studied extensively. High magnitudes of impact forces induced by wheel defects can cause severely flexible vibrations of wheelset axles, and then contribute to the considerable increase in the stress states of wheelset axles, which can impose extremely threatens to the running safety of rail vehicles and reduce the residual lifetime of a wheelset axle in the occurrences of initial cracks. Consequently, the stress states and damage tolerances of a wheelset axle in the presence of wheel defects are discussed in this study by using a coupled vehicle/track model integrating with a flexible wheelset model. In this model, a rigid-flexible coupled vehicle dynamic model treating the wheelset as a flexible body is formulated in the Simpack platform. The track, modeled as a Timoshenko beam discretely supported on a flexible track slab in the Simulink platform, is subsequently integrated to the multibody dynamic model of the vehicle in the Simpack platform through the co-simulation interface SIMAT (Simpack-Matlab co-simulation).

2. Coupled vehicle/track dynamic model

The coupled vehicle/track dynamic model is formulated by a rigid-flexible coupled vehicle dynamic model and a slab track model. The commercial software SIMPACK is employed to develop the rigid-flexible coupled vehicle dynamic model together with a rotating flexible wheelset model. The slab track model is formulated by Simulink using the modal synthesis method. The rigid-flexible coupled vehicle dynamic model and the slab track are then integrated using a communication module SIMAT, as illustrated in Fig. 1.

2.1 Modelling of flexible wheelset

The wheel/rail impact force could cause the elastic deformation of the wheelset. Such elastic deformations of wheelset can significantly affect the estimations of wheel/rail contact forces and axle box accelerations. A rotating flexible wheelset model, developed by using the modal synthesis method, is thus integrated into the vehicle dynamic model to represent the dynamic responses of wheelset more realistically. In the model, the reference frame that describes the translational and rotational motions of wheelset is employed to represent the flexible wheelset, as shown in Fig. 2(a).

The elastic deformations of the wheelset due to the external forces can be defined with respect to this frame, which can be given by [22]

$$\mathbf{d}(\mathbf{c}, t) = \mathbf{c} + \mathbf{u}(\mathbf{c}, t) \tag{1}$$

where $\mathbf{d}$ is the displacement vector from the reference frame to the material point after loading, $\mathbf{c}$ indicates the position of the material point in the un-deformed state, $\mathbf{u}$ is the elastic displacement vector associated with the reference position $\mathbf{c}$ and the time t. Using the modal approach the elastic deformation $\mathbf{u}(\mathbf{c}, t)$ can be expressed as

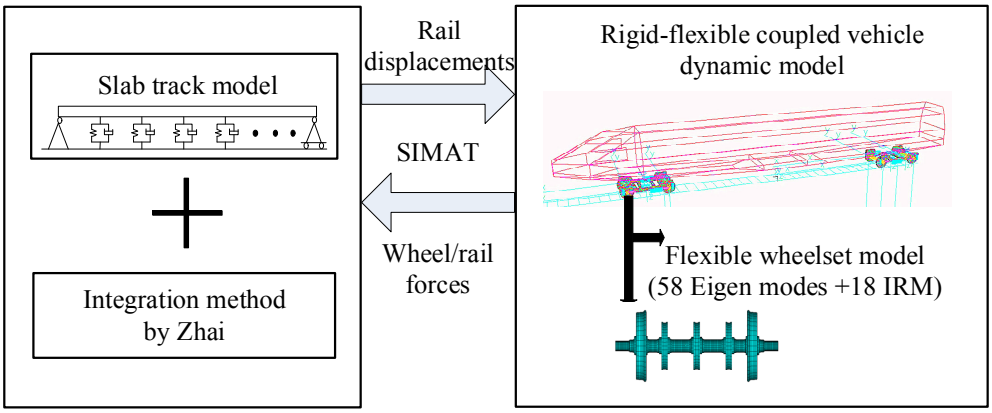

Fig. 1. Schematic of coupled vehicle/track dynamic model.

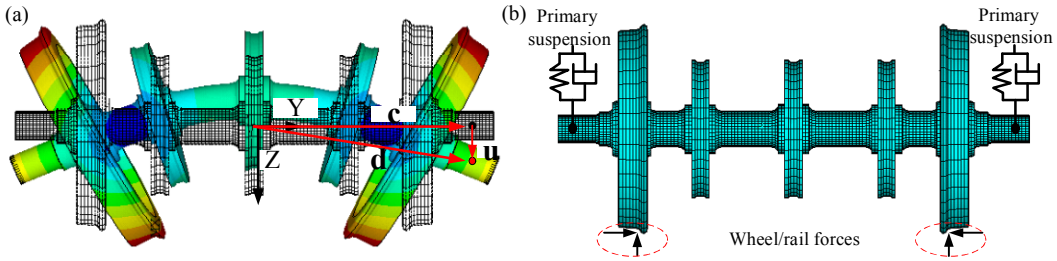

Fig. 2. Modelling of flexible wheelset.

$$\mathbf{u}(\mathbf{c}, t) = \mathbf{\Phi}(\mathbf{c})\, q_w(t) \tag{2}$$

where $q_w(t)$ denotes the generalized coordinates of the elastic deformation, $\mathbf{\Phi}(\mathbf{c})$ is the time-invariant modal shape matrix, which can be obtained from the finite element model of wheelset. In this study, the finite element program ANSYS is utilized to build the FEM model of wheelset using the element type of Solid 45 provided by ANSYS, which leads to 53524 nodes and 43764 elements totally, as illustrated in Fig. 2(b). The eigen-mode of wheelset is calculated by the modal analysis. Since the high frequency vibrations induced by the wheel defects are the focus, 58 vibration modes of wheelset are taken into account considering the highest frequency occurring at frequency of 2533 Hz, as shown in Fig. 3. To consider the local deformation caused by the external forces (wheel/rail contact forces and primary suspensions) static modes are taken into account as additional shape functions [23]. The static modes can be considered as either Frequency response modes (FRM) or Inertial relief modes (IRM). In this study, the inertial relief modes are used to describe the static modes, which results in 12 IRMs for the primary suspension and 6 IRMs for the wheel/rail contact forces in the model.

Using the modal approach equations of motion for the flexible wheelset model can be expressed as,

$$\ddot{q}_w - 2\Omega\tilde{G}\dot{q}_w + (\tilde{K} + \Omega^2\tilde{C})q_w = Q_q + \Omega^2\tilde{L} \tag{3}$$

where Ω is the spinning angular velocity of the wheelset, $\tilde{G}$ expresses the gyroscopic matrix, $\tilde{K}$ is a diagonal matrix containing the square of the natural frequencies of wheelset, $\Omega^2\tilde{C}q_w$ and $\Omega^2\tilde{L}$ denote the centripetal acceleration due to rotation: The former is associated with the deformation of the solid and the latter with the undeformed shape, Q_q is the generalized force vector.

The displacements of the wheelset at any material point, thus, can be given as

$$\mathrm{u}=\sum_{j=1}^{NM}\Phi_j q_j = [\mathbf{\Phi}]\{q\} \tag{4}$$

where u is the displacement of the wheelset at the desired point, Φ_j is the jth mode vector, q_j is the modal coordinates for the jth mode, NM is the total number of modes considered in the flexible wheelset.

The stress σ of the wheelset axle at any given point can be written as

$$\{\sigma\} = [\mathbf{D}]\{\varepsilon\} = [\mathbf{D}][\mathbf{B}]\{q\} \tag{5}$$

$$[\mathbf{B}] = [\mathbf{L}][\mathbf{\Phi}] \tag{6}$$

where $\mathbf{D}$ is the elasticity matrix, $\mathbf{L}$ is the linear operator relating the strain ε and the displacement u, $\mathbf{\Phi}$ is the modal vector matrix.

2.2 Rigid-flexible coupled vehicle dynamic model

The Simpack platform is employed to establish the rigid-flexible coupled vehicle dynamic model since its feasibility

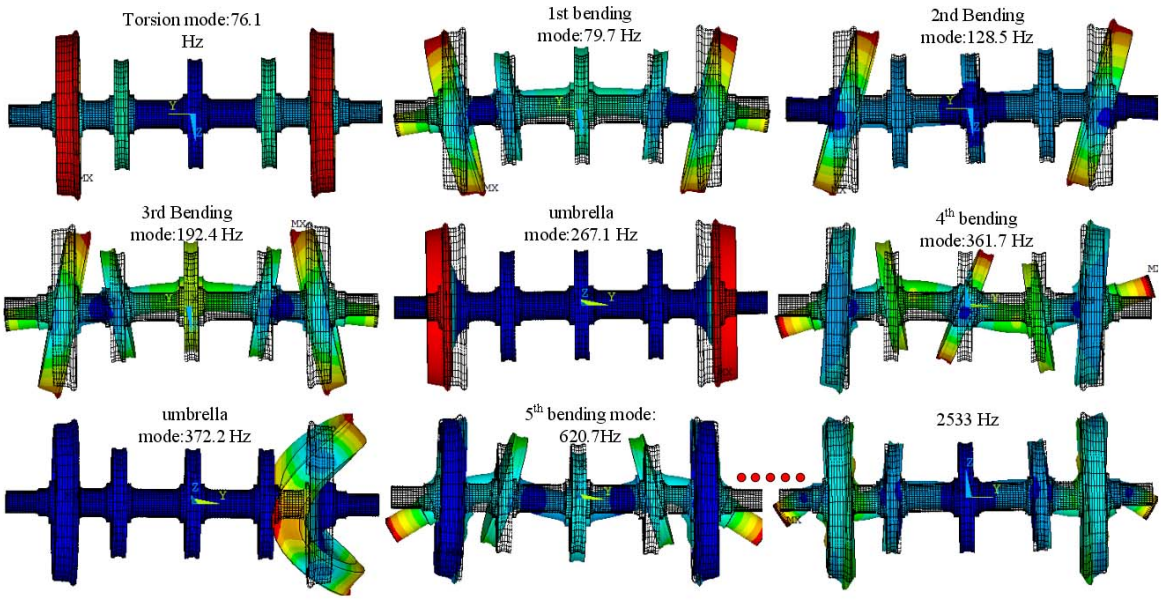

Fig. 3. Vibration modes considered in the flexible wheelset.

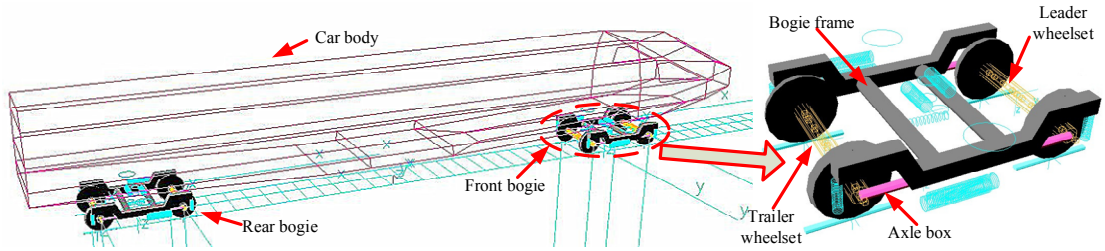

Fig. 4. Vehicle dynamic model.

has been widely accepted by researchers. The vehicle is a typical High speed train model consisting of a car body, two bogie frames, four wheelset and eight axle boxes, as shown in Fig. 4. The car body rests on two bogies through secondary suspensions, and the wheelsets are connected to the bogie frame by the primary suspensions in the vertical direction and the axle boxes via the rubber elements in the longitudinal direction. The primary and secondary suspension are modelled as linear springs in parallel with linear dampers acting in three directions. In the model, the car body and the bogie frame are modelled as rigid bodies with 6 degrees of freedom, and only the pitch motion with respect to the wheelset is taken into account for the axle boxes, while the wheelsets are established as the rotating flexible wheelsets using the aforementioned approach.

2.3 Slab track model

The slab track system that consists of rails, fastener system, track slab, Cement asphalt mortar (CAM) layer and concrete roadbed has been widely adopted in the high-speed railway line due to its low maintenance characteristics, as shown in Fig. 5. Therefore, the slab track model is taken into account in this study, in which the rails and the track slab are, respectively, formulated by the Timoshenko beam theory and the finite element method, while the fastener system and CAM layer are established as a set of linear spring-damper elements. In this study, the lateral, vertical and rotation motions of the rail are included, whereas, only the vertical motion of the track slab is taken into consideration.

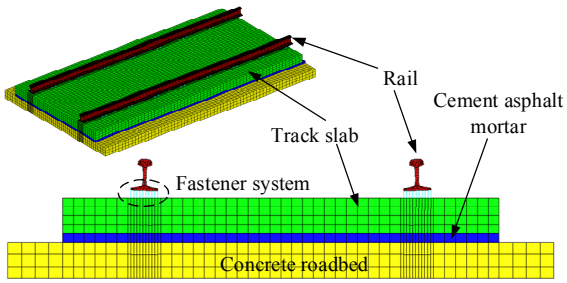

Fig. 5. Slab track system.

2.3.1 Rail model

The loads acting on the rail can be illustrated in Fig. 6. On the basis of the Timoshenko beam theory [24], the equation of

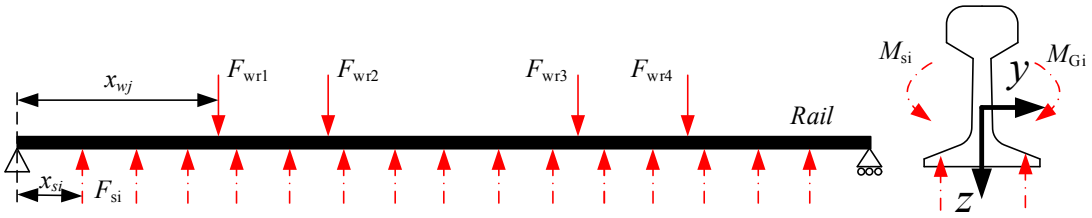

Fig. 6. Rail model.

motions of rails can be expressed as below:

Vertical deflections of rails:

$$m\frac{\partial^2 z(x,t)}{\partial t^2}+\kappa_z \mathrm{GA}\left[\frac{\partial \psi_z(x,t)}{\partial x}-\frac{\partial^2 z(x,t)}{\partial x^2}\right] =-\sum_{i=1}^{N_s}F_{szi}\delta(x_{si})+\sum_{j=1}^{N_w}F_{wrzj}\delta(x_{wj}) \tag{7}$$

$$\rho I_y\frac{\partial^2 \psi_z(x,t)}{\partial t^2}+\kappa_z \mathrm{GA}\left[\psi_z(x,t)-\frac{\partial z(x,t)}{\partial x}\right] -\mathrm{EI}_y\frac{\partial^2 \psi_z(x,t)}{\partial x^2}=0\,. \tag{8}$$

Lateral deflection of rails:

$$m\frac{\partial^2 y(x,t)}{\partial t^2}+\kappa_y \mathrm{GA}\left[\frac{\partial \psi_y(x,t)}{\partial x}-\frac{\partial^2 y(x,t)}{\partial x^2}\right] =-\sum_{i=1}^{N_s}F_{syi}\delta(x_{si})+\sum_{j=1}^{N_w}F_{wryj}\delta(x_{wj}) \tag{9}$$

$$\rho I_z\frac{\partial^2 \psi_y(x,t)}{\partial t^2}+\kappa_y \mathrm{GA}\left[\psi_y(x,t)-\frac{\partial y(x,t)}{\partial x}\right] -\mathrm{EI}_z\frac{\partial^2 \psi_y(x,t)}{\partial x^2}=0\,. \tag{10}$$

Torsion deflection of rails,

$$\rho I_0\frac{\partial^2 \phi(x,t)}{\partial t^2}+\mathrm{GK}\frac{\partial^2 \phi(x,t)}{\partial x^2}=-\sum_{i=1}^{N_s}M_{si}\delta(x_{si}) +\sum_{j=1}^{N_w}M_{Gj}\delta(x_{wj}) \tag{11}$$

where z, y and ϕ are, respectively, the vertical, lateral and torsion deflection of rail, ψ_z and ψ_y are the rotation deflection of the cross section with respect to the y and z axis, m is the mass of rail per unit length, ρ is the density, A is the area of cross section for the rail, G is the shear modulus, E is the Young's modulus, I_y and I_z are the second moments of area for rail cross section around the y and z axis, I_0 is the polar moment of inertia of the rail cross section, κ_y and κ_z are the lateral and vertical shear coefficients, F_{szi}, F_{syi} and M_{si} denotes the vertical, the lateral forces and thee moments between the rail and ith support, F_{wrzj}, F_{wryj} and M_{Gj} represents the vertical and lateral wheel/rail forces and the moments acting on the rail,

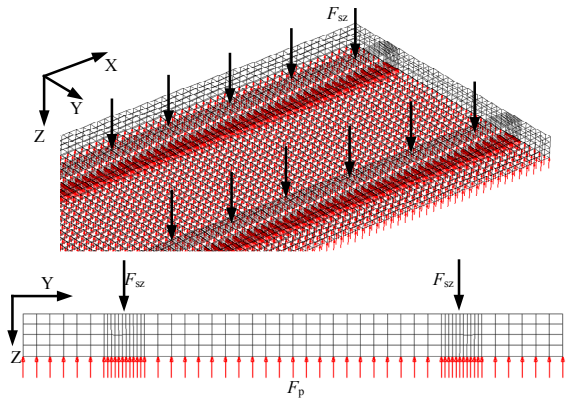

Fig. 7. Slab track model.

$\delta(x_{si})$ is the Dirac delta function, x_{si} is the coordinate of ith support, x_{wj} is the coordinate of wheel j, N_s and N_w are the number of support and wheelset. According to the modal superposition method and normalized mode shape function of rail, the deflection of rail can be expressed

$$z(x,t)=\sum_{k=1}^{NMZ}Z_k(x)q_{zk}(t)\;;\;\psi_z(x,t)=\sum_{k=1}^{NMZ}\Psi_{zk}(x)\omega_{zk}(t)$$
$$\phi(x,t)=\sum_{k=1}^{NMT}\Phi_k(x)q_{Tk}(t)\;;\;y(x,t)=\sum_{k=1}^{NMY}Y_k(x)q_{yk}(t)$$
$$\psi_y(x,t)=\sum_{k=1}^{NMY}\Psi_{yk}(x)\omega_{yk}(t) \tag{12}$$

where the $q_{zk}(t)$, $q_{yk}(t)$ and $q_{Tk}(t)$ are, respectively, the modal coordinates in vertical, lateral and torsion direction, $\omega_{zk}(t)$ and $\omega_{yk}(t)$ are modal coordinates about the y and z axis, $Z_k(x)$, $Y_k(x)$ and $\Phi_k(x)$ denote the mode shape functions of rail for the vertical, lateral and torsion, respectively. $\Psi_{yk}(x)$ and $\Psi_{zk}(x)$ are the kth mode shape functions of the rail cross-section rotation about the y and z axis. In this study the mode shape functions of simply supported beam are taken into account [25].

2.3.2 Slab track model

According to the finite element method, the equations of motion for slab track model in the global coordinate system can be expressed as [25]

$$[M]\{\ddot{x}\}+[C]\{\dot{x}\}+[K]\{x\}=\{F_{sz}\}+\{F_p\} \tag{13}$$

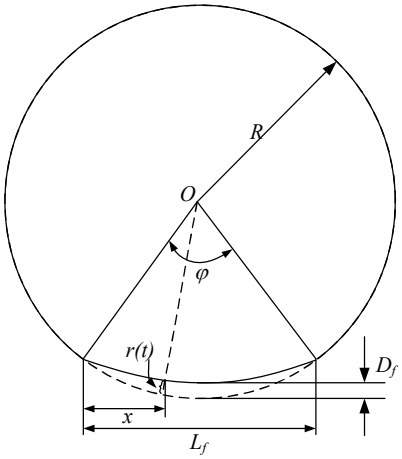

Fig. 8. Haversine wheel flat.

where [*M*], [*C*] and [*K*] denote the mass matrix, damping matrix and stiffness matrix, respectively. $\{F_{sz}\}$ is the force between the rail and slab, $\{F_p\}$ expresses the support forces of slab. Using the modal superposition principle, the Eq. (22) can be transformed to a set of uncoupling equations

$$M_n\ddot{X}_n + C_n\dot{X}_n + K_nX_n = P_n \tag{14}$$

where X_n is the modal coordinates, M_n, C_n, K_n and P_n are the normal coordinate generalized mass, damping, stiffness, and load for *n*th mode, respectively. The displacement of the slab track can be evaluated through the modal superposition method, as follows:

$$\{x\} = \sum_{n=1}^{N_{mode}} \{\phi\}_n X_n = \{\Phi\}\{X\}_i . \tag{15}$$

2.4 Wheel/rail contact model

The profiles of the wheel and the rail adopted in this model are, respectively, S1002CN and Rail 60. Fastsim [26] is employed to evaluate the lateral and longitudinal creep forces between the wheel and the rail. The normal forces of wheel/rail interface are evaluated using the Hertzian contact theory [27].

The wheel flat can be classified into the new formed wheel flat and the haversine wheel flat [4]. The new formed wheel flat with sharp edges tends to be more round as the wheel continuously operates, and then transfers to the haversine wheel flat. Consequently, the haversine wheel flat is employed to describe the wheel flat, as shown in Fig. 8. The variations of the radius in the contact point *r*(t) can be expressed as:

$$r(t) = \frac{1}{2}D_f\left[1-\cos(2\pi x / L_f)\right] \tag{16}$$

where D_f is the flat depth associated with the wheel radius *R*, and can be given as

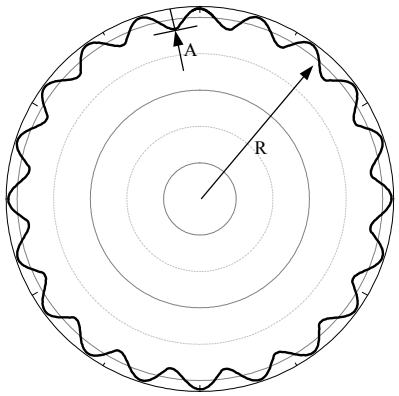

Fig. 9. Wheel ploygonalization.

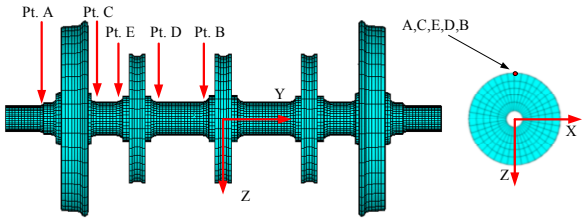

Fig. 10. 5 Points considered in the wheelset axle.

$$D_f = L_f^2 / (16R) . \tag{17}$$

An ideal polygonal wheel can be described through harmonic deviations, as shown in Fig. 9, which can be expressed as:

$$\begin{cases} x = (R + A\sin N\varphi)\sin\varphi \\ y = (R + A\sin N\varphi)\cos\varphi \\ \varphi \in [0, 2\pi] \end{cases} \tag{18}$$

where *A* denotes the amplitude of the wheel polygnoalization, φ defines the wheel rotation angle, *N* describes the order of polygon wear, which is considered as 20 in this study.

3. Validations of stress states of wheelset axle through the finite element method

In this study, the stress states in the wheelset axle are evaluated from the modal stress using the modal stress recovery method [28]. Its accuracy largely depends on considered vibration modes in the flexible wheelset model. The finite element method is thus employed to validate the feasibility of the flexible wheelset model that used in the estimations of stress states of the wheelset axle. The stresses in y direction of 5 points locating at 5 critical sections of the wheelset axle are taken into consideration to identify the bending stresses of the wheelset axle due to wheel defects, as shown in Fig. 10.

For the purpose of validation, the dynamic stresses of the wheelset axle showed in Fig. 11 are estimated without consid-

Table 1. Comparisons in the stress states of the wheelset axle (MPa).

Stress states (MPa)	Point A	Point B	Point C	Point D	Point E
Modal method	25.2	24.3	32.1	25.5	26.3
FEM	29.0	29.7	32.6	29.8	29.5

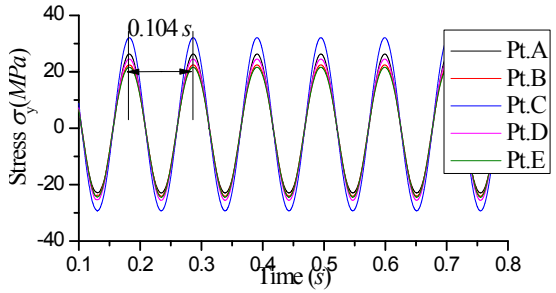

Fig. 11. Dynamic stresses of wheelset axle.

eration of wheel defects and track irregularities, which usually referred to the quasi-static stress states under the static wheel loads. The quasi-static stress states of wheelset axle express a waveform of sinusoid wave due to wheel rotations, and fluctuates at a period of 0.104 s attributed to the wheel rotation frequency at a speed of 100 *km/h*. In addition, the maximum and minimum points of dynamic stresses represent two different stress states at selected points, namely, the tension and compression stress states. Alternatively, the quasi-static stress states of a wheelset axle under the static wheel loads can also be evaluated using the finite element method through the static analysis. The comparisons in the stress states of the wheelset axle obtained by the modal stress and the finite element method are summarized in Table 1. It can be seen that the quasi-static stresses at Point A, B, D and E obtained by the modal approach are a little bit smaller than the FEM' results due to the truncation errors of mode frequencies for the flexible wheelset model. In this study the considered mode frequencies of the wheelset reach up to 2533 Hz to cover most interested frequencies ranges, thus, these errors are accepted in our theoretical study to lead to more conservative results.

4. Stress states of wheelset axle induced by wheel flats

In the case of wheel flats, the wheel flats are considered at the same position of each side of wheels in the simulations. Fig. 12 indicates the dynamic stresses of the wheelset axle caused by a flat with size of L_f = 60 *mm* at a speed of 100 *km/h*. It can be observed that the flats-induced impact forces impose significant fluctuations in the troughs of dynamic stresses in comparison with the quasi-static stress states (results in Fig. 11). It implies that the stress states of selected points experience the compression states during the impacts of wheel flats, while the tension stress states also can be obsevered associated with positions of the selected points in a wheelset axle. The results also show that Pt. A, Pt. C and Pt. E experience more severe fluctuations compared to those of Pt. B and Pt. D, which means that the Sec. A, C and E are more sensitive to the flats-induce impact forces.

To exhibit the effects of wheel flats on flucutations of dynamic stresses in the wheelset axle, comparison analyses for the case of L_f = 60 mm between the flats-induced dynamic stresses and the quasi-static stress are plotted in polar coordinate system, as shown in Fig. 13. Owing to the wheel flats-induced impact forces the dynamic stresses of wheelset axle express notable fluctuations around the quais-static stress states. Moreover, the peak-peak fluctuation amplitudes around the quais-static stress state for the Pt. A and Pt. E reach about 23.2 MPa and 21.2 MPa, respectively.

The stress states of the wheelset axle involving different flat sizes and forward speeds are illustrated in Fig. 14. As the results indicate that the stress variations of wheelset axle are significantly dependent upon vehicle speeds and wheel flat sizes. In the case of L_f = 60 *mm*, the maximum stress amplitudes of Pt. A, Pt. C and Pt. E reach about 32.2 *MPa*, 36.5 *MPa* and 33.1 *MPa*, respectively.

The stress increment ratio, defined as the stress increment in a wheelset axle over the quais-static stress state, is used to exhibit the effects of vehicle speeds and wheel flat sizes on the stress variations of wheelset axleas shown in Fig. 15. It can be seen that when the size of wheel flat exceeds 40 *mm*, the stress increment ratios of Point A and Point C are extremly sensitive to the wheel flat sizes, and increase sharply with the wheel flat sizes. The stress increment ratios of Point A and Point C reach the peak of 23.8 % and 12.4 % in the case of L_f = 60 *mm*. For Point E, the stress increment ratios increase monotonously as the size of wheel flat increases, and reach the maximum value of 35.1 % in the speed range 150 ~ 200 *km/h* for the case of L_f = 60 *mm*.

On the basis of above investigations, the wheel flats are identified as the local effects on the dynamic stresses of wheelset axle in one wheel revolution. Nevertheless, it also can result in increases in the stress states of the wheelset axle up to 35.1% stress increment ratio for the case of L_f = 60 *mm*. Although the maximum fluctuation amplitudes of wheelset axle stress induced by wheel flats are still lower than the fatigue limits defined by EN 13103/13104 [29] in our considered situation, it could raise the concerns on the damage tolerances of the wheelset axle in the occurrences of initial cracks. Therefore, it is neassary to take the damage tolerances of a wheelset alxe into considerations in the removal criteria of the wheel flats.

5. Stress states of wheelset axle induced by wheel polygonalization

Compared with wheel flats, wheel polygonalization is a kind of periodic wear along the wheel circumference, which could generate high magnitudes and high frequencies impact forces at the wheel/ rail interfaces and impose extremely threaten to the running safety of railway vehicles [21]. The wheel polygonalization with 20 orders was recently observed

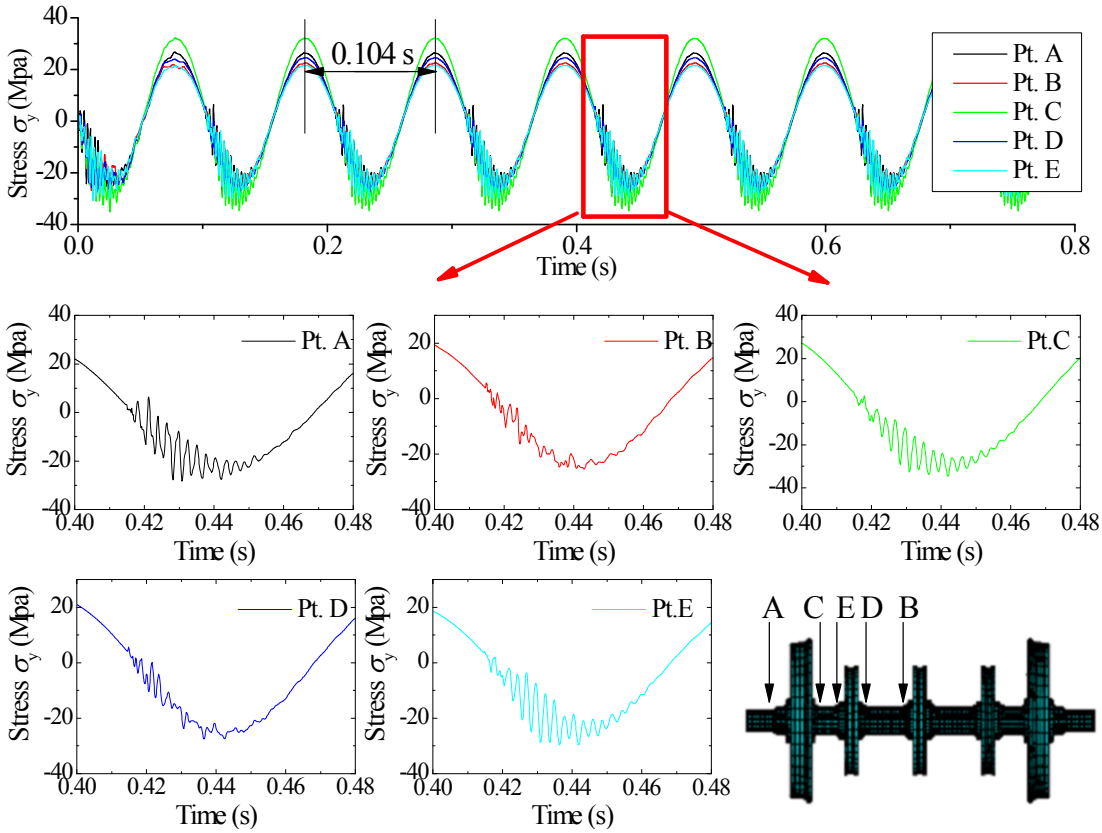

Fig. 12. Dynamic stress of wheelset axle in the case of L_f = 60 mm in case 3.

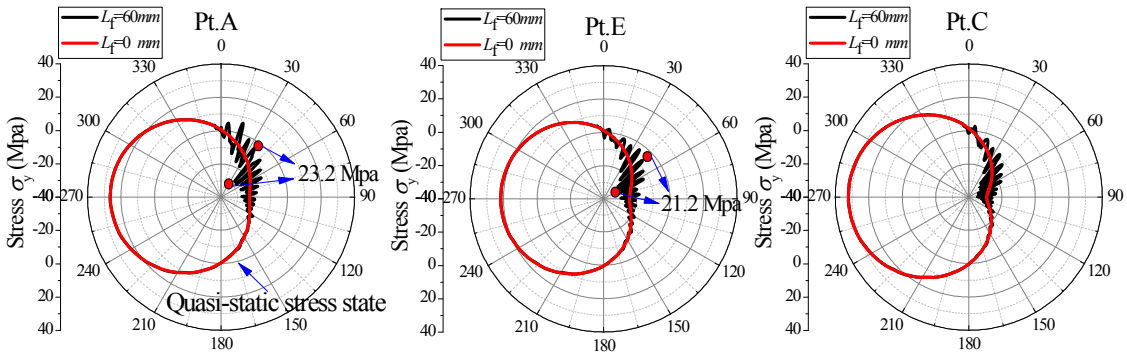

Fig. 13. Comprison analyses between the flats-induced dynamic stress and quasi-static stress states for the case of L_f = 60 mm.

in some railway vehicles, which gives rise to about 576 *Hz* high frequency vibrations at wheel/rail interfaces when the vehicle operates at a speed of 300 *km/h*. Such high frequency vibrations impose tremendous influences on the safety of vehicle/track system. The wheels with the 20th order polygonalization are thus taken into account in this section.

Through the coupled vehicle/track dynamic model incorporating with the flexible wheelset model, the dynamic stresses of the wheelset axle in the presence of wheel polygonalizations (0.16 *mm*) are evaluated at a speed of 180 *km/h*, as shown in Fig. 16. It can be observed from Fig. 16(a) the dynamic stresses of the wheelset axle experience severe fluctuations due to the wheel polygonalization-induced impact loads. Figs. 16(b)-(f) illustrate the effects of wheel polygonalization on the dynamic stress in the wheelset axle through comparing to the quasi-static stress in the polar coordinate system. The results indicate that the dynamic stresses of Point A, C and E are very sensitive to the wheel polygonalization-induced impact forces, and the peak-peak fluctuation amplitude reach a maximum value of 35.9 *MPa* at Point A.

Fig. 17 illustrates the maximum stress of the wheelset axle considering different wheel polygonalization amplitudes and vehicle forward speeds. The results show significant increases in the stress states of the wheelset axle in the speed range

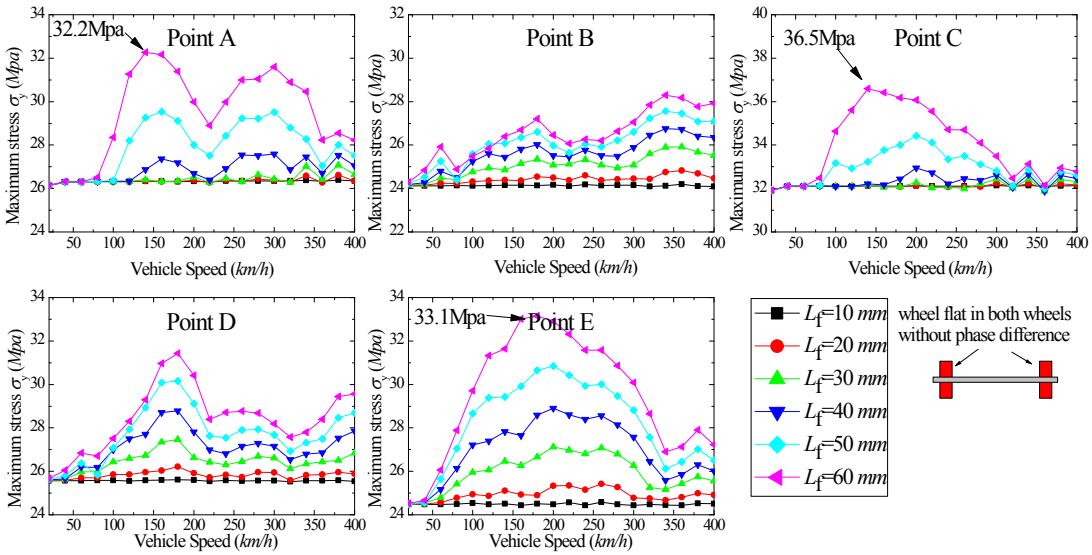

Fig. 14. Stress states of wheelset axle at different speeds.

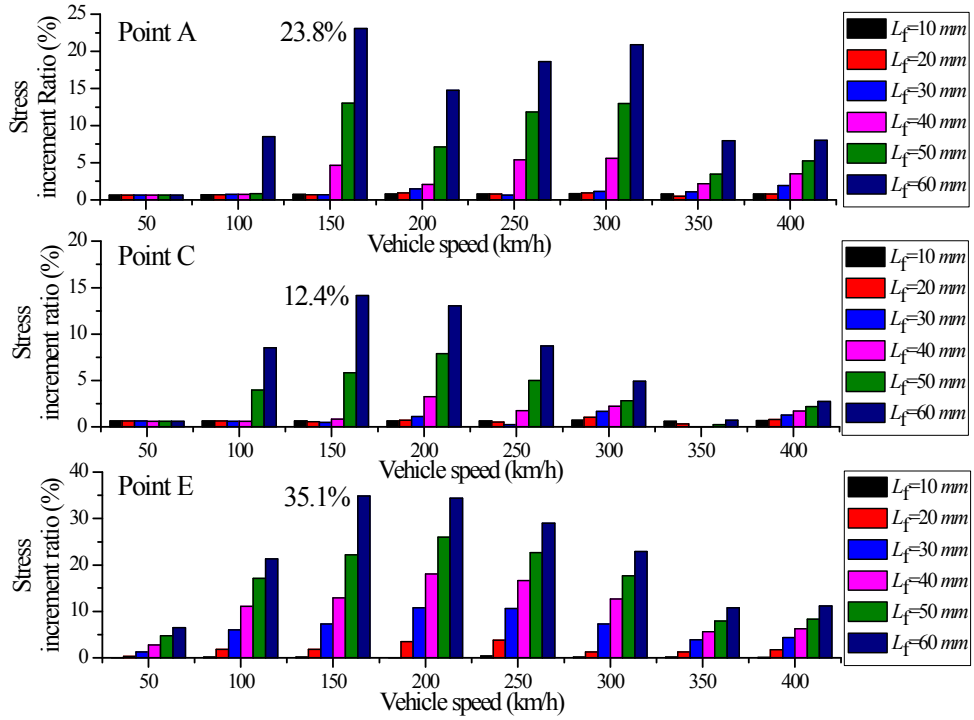

Fig. 15. Stress increment ratios of the wheelset axle due to wheel flats.

120~240 *km/h* for the Point A, C, E. The stresses σ_y reaches the maximum value at the speed of about 180 *km/h*, and then decrease with the continuously increased vehicle speeds. Since the passing frequency of the 20th order wheel polygonalzaition at the speed of 180 *km/h* is about 345.9 *Hz* closing to the natural frequency of the wheelset 361.7 *Hz* (in Fig. 3), these increases in the wheelset axle are mainly attributed to the structural resonance of the wheelset in the speed range 120~240 *km/h*. Similarly, the increases for Point B and D above the speed of 160 *km/h* are also induced by resonance vibrations of the wheelset.

The relationships between the maximum stress increment ratios and wheel polygonalization amplitudes are given in Fig. 18. It can be seen that in the considered speed range (60~380 *km/h*) the maximum stress increment ratios increase monotonously with the amplitudes of wheel polygonalization, and reach about 100% for the Point B and D at the wheel polygonalizaiton amplitude of 0.1 *mm*. Such high dynamic stresses impose extremely threaten to the safety of vehicles and lower the damage tolerances of the wheelset axle in the presence of

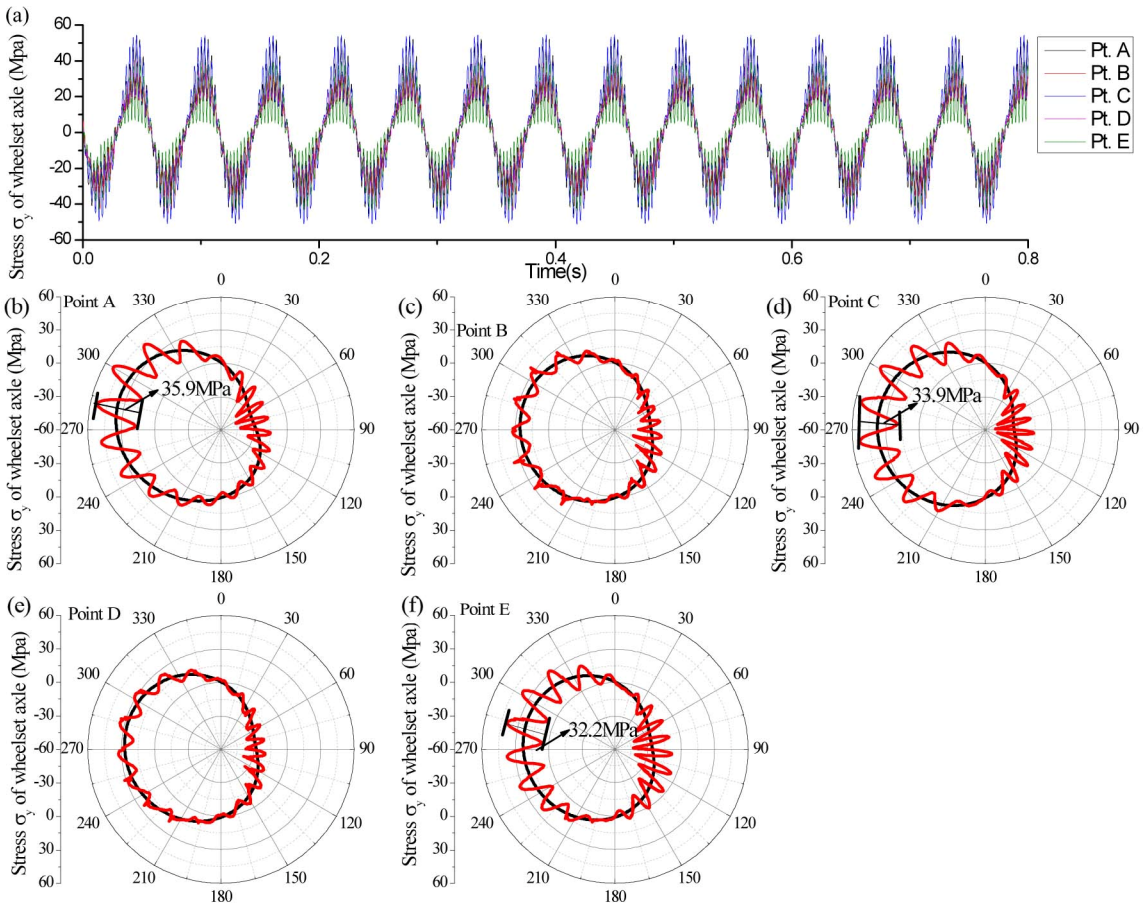

Fig. 16. Dynamic stresses of wheelset axle due to wheel polygonalization at speed of 180 *km/h*.

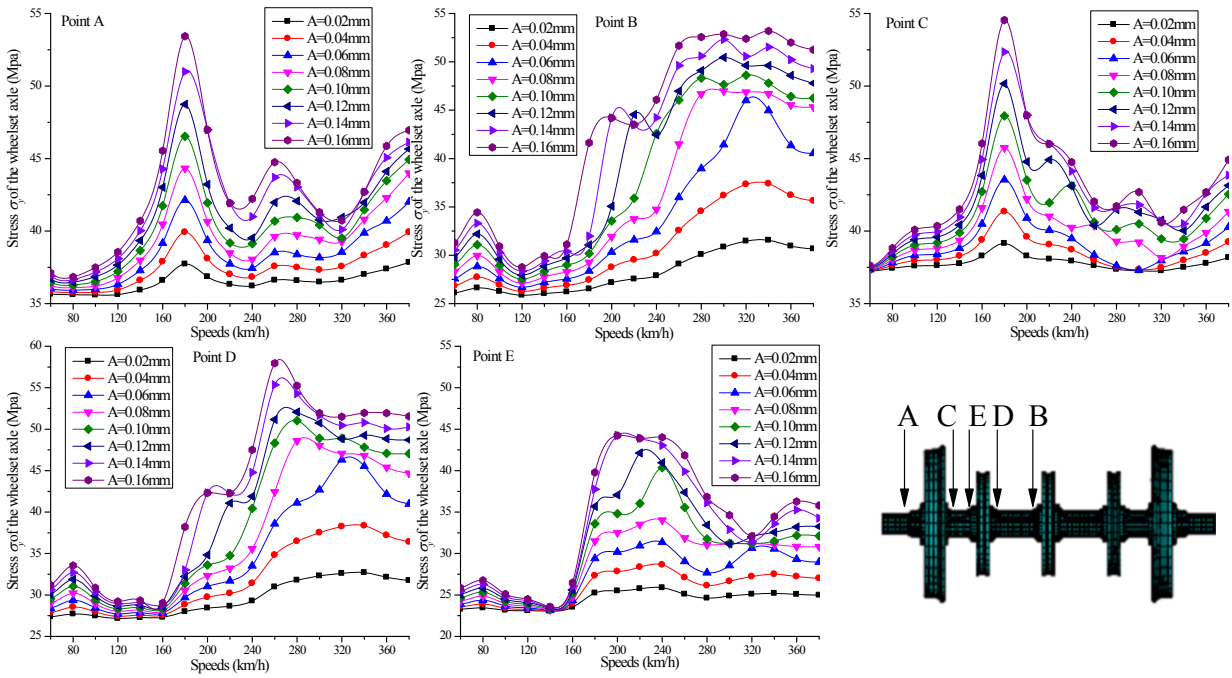

Fig. 17. Stress states of the wheel axle caused by wheel polygonalizations.

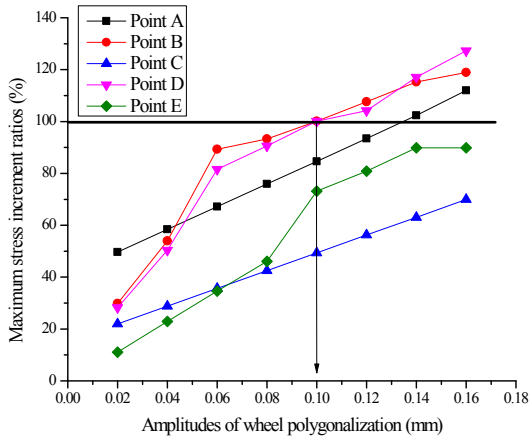

Fig. 18. Relationship between maximum stress increment ratios and amplitude of wheel polygonalization.

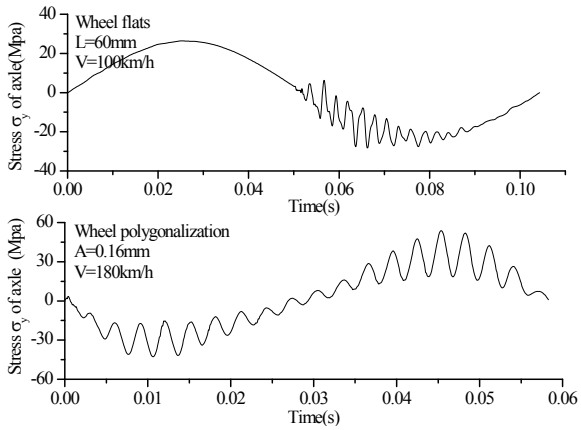

Fig. 19. Typical stress spectrum of wheelset axle induced by wheel defects (flats, polygonalization).

wheel polyonalization.

6. Damage tolerances of wheelset axle in the presence of wheel defects

According to the above investigations, the wheel defects-induced stress amplitudes are smaller than the fatigue limits 240 *MPa* defined by EN standards, while it could contribute to the propagations of initial cracks in the wheelset axle. The damage tolerances of wheelset axle in the presence of wheel defects are evaluated to exhibit the effects of wheel defects on the residual lifetime of a wheelset axle with an initial crack.

A typical stress spectrum of a wheelset axle due to wheel defects consist of quasi-static stresses and dynamic components, as shown in Fig. 19. Quasi-static stresses are regarded as results of wheel rotations under static wheel loads, while the dynamic components around quasi-static stresses are mainly introduced by the wheel defects-induced impact forces. Fig. 20 shows load cycles during a wheel revolution obtained using the rail-flow counting method. In the load cycles spectrum, there are two types of load cycles, namely, wheel de-

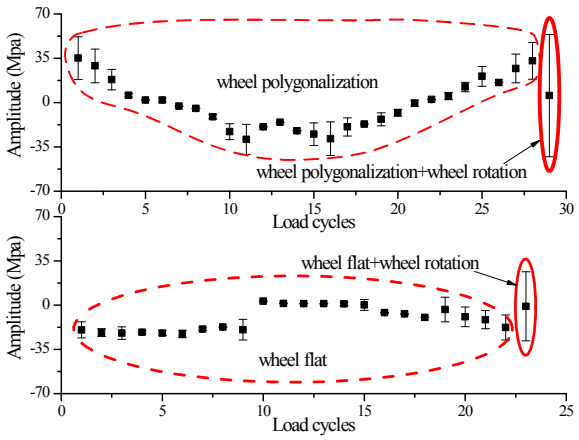

Fig. 20. Typical load cycles during a wheel revolution obtained by rail-flow counting.

fects-induced load cycles and wheel rotation- defects-induced load cycles. Wheel rotation-defects-induced load cycles are considered as the results of superposing the load cycles caused by wheel defects and wheel rotations, consequently, the amplitudes of wheel rotation-defects- induced load cycles are apparently larger than wheel defects-induced load cycles. Meanwhile, the wheel rotation-defects-induced load cycles are characterized by large amplitudes and small mean values, and the stress ratio R is close to -1, which may contribute to the propagation of initial cracks in a wheelset axle.

The crack propagation algorithm used in this study is based on the NASGRO algorithm [30], which is given by:

$$\frac{da}{dN} = C\left[\left(\frac{1-f}{1-R}\right)\Delta K\right]^n \frac{\left(\frac{1-\Delta K_{th}}{\Delta K}\right)^p}{\left(\frac{1-K_{\max}}{K_{crit}}\right)^q} \tag{19}$$

$$\Delta K_{th} = \Delta K_{th0} \frac{\sqrt{\frac{a}{a+a_0}}}{\left[\frac{1-f}{(1-A_0)(1-R)}\right]^{(1-C_{th}R)}} \tag{20}$$

where a is crack length, N is number of load cycles, C, n, p, q are empirical coefficients, R is stress ratio, ΔK is the Stress-intensity-factor (SIF) range, ΔK_{th} is the threshold of SIF, $K_{\max}$ is the SIF of the maximum loading force in the cycle, K_c is critical value of SIF referred to fracture toughness, f is Newman's function describing closing of the crack, a_0 structural crack length that depends on the material grain size. ΔK_{th0} threshold SIF at $R = 0$, C_{th} curve control coefficient for different values of R. In this study, the material of the axle is considered as steel, the initial length of crack is 2 mm, the threshold value of SIF ΔK_{th} is taken as $2MPa\sqrt{m}$, $q = 0.001$, $C_{th} = -0.029$, $C = 4.53\times10^{-10}$, $n = 2.09$, $p = 1.3$.

Based on the above wheel defects-induced load cycles, the

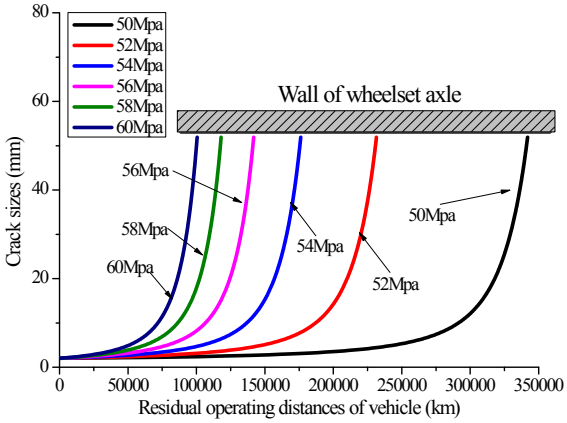

Fig. 21. Crack growth in the presence of wheel polygonalizations.

Stress-intensity-factors (SIF) due to the wheel flats are less than the threshold value of SIF ΔK_{th}, which means that the initial crack would not propagate due to the flats-induced impacts in our considered situations. Therefore, the case of wheel polygonalization is only taken into consideration in this section, meanwhile, the wheel rotation-defect-induced load cycles are only considered since the wheel defect-induced load cycles are small and cannot result in the propagations of crack. Consequently, the analyses of damage tolerances of a wheelset axle in the presence of wheel polygonalization can be conservatively simplified as a case of wheelset axle under constant amplitude load cycles.

Through the NASGRO equations, the crack growth in the wheelset axle is evaluated as a function of the residual operating distances of vehicle in the presence of wheel polygonalizations, as shown in Fig. 21. It can be seen that with the increase in operating distances of vehicle the size of crack in the wheelset axle propagate rapidly, and the amplitudes of load cycles show significant influences on the propagations of crack and remaining operating distances of the wheelset axle. Therefore, a reasonable inspection strategy for a wheelset axle should be established to avoid the wheel polygonalization-induced axle fracture in the presence of wheel polygonalizations.

7. Conclusions

In this paper, a comprehensive coupled vehicle/ track dynamic model integrating with a flexible wheelset model is formulated to investigate the stress states of the wheelset axle in the presences of wheel defects. The stress states of the wheelset axle are evaluated by using the modal stress recovery method, and validated by the finite element method. The validation results show a little bit errors in the stress states that obtained by the model stress recovery method due to the truncation errors of mode frequencies for the flexible wheelset model, which lead to more conservative results. The wheel defects-induced impact forces could results in severe fluctuations in the stress around the quasi-static stress of wheelset axle. For the case of wheel flats, the stress increment ratio of the wheelset axle become sensitive to the size of flat when the flat size exceeds 40 mm. In addition to wheel polygonalizations, the resonance of wheelset axle can be excited, which leads to the notably increases in the stress states of the wheelset axle. Moreover, the maximum stress increment ratios increase monotonously with the amplitudes of wheel polygonalization and could reach up to 100 %. The damage tolerances of the wheel axle evaluated by NASGRO equations indicate that the wheel polygonalization-induced impact forces impose significant influences on the residual operating distances of a wheelset axle in the occurrences of initial crack in the axle. The residual lifetime of the wheelset axle decrease considerably with the increase in stress amplitudes. Whereas, further experimental investigations are needed to validate the wheel defects-induced load cycles and the residual lifetime of wheelset axle in the presence of wheel polygonalizations.

Acknowledgment

The present work has been supported by the National Basic Research Program of China (2011CB711106), 2014J008-A, 2014J008-B and 2012TPL-T03.

References

[1] J. C. O. Nielsen and A. Johansson, Out-of-round railway wheels-a literature survey, *I. Mech. E, Part F: Journal of Rail and Rapid Transit*, 214 (2) (2000) 79-91.

[2] M. R. U. A. Uzzal, *Role of railway vehicle-track system and design parameters on flat-induced impact load,* Concordia University, Montreal, Canada (2007).

[3] J. Jergéus, Full-scale railway wheel flat experiments, *I. Mech. E, Part F: Journal of Rail and Rapid Transit*, 213 (1) (1998) 1-13.

[4] K. Hou, J. Kalousek and R. Dong, A dynamic model for an asymmetrical vehicle/track system, *Journal of Sound and Vibration*, 267 (3) (2003) 591-604.

[5] T. Snyder and D. H. Stone, Wheel flat and out-of-round formation and growth, *Proceedings of the 2003 IEEE/ASME Joint Rail Conference*, Chicago, USA (2003).

[6] J. C. O. Nielsen and A. Igeland, Vertical dynamic interaction between train and track influence of wheel and track imperfections, *Journal of Sound and Vibration*, 187 (5) (1995) 825-839.

[7] S. G. Newton and R. A. Clark, An investigation into the dynamic effects on the track of wheelflats on railway vehicles, *Journal of Mechanical Engineering Science*, 21 (4) (1979) 287-297.

[8] R. G. Dong and S. Sankar, A finite element model of railway track and its application to the wheel flat problem, *I. Mech. E, Part F: Journal of Rail and Rapid Transit*, 208 (1) (1994) 61-72.

[9] J. Bian, Y. Gu and M. H. Murray, A dynamic wheel–rail impact analysis of railway track under wheel flat by finite

element analysis, *Vehicle System Dynamics*, 51 (6) (2013) 784-797.
[10] R. V. Dukkipati and R. Dong, Impact loads due to wheel flats and shells, *Vehicle System Dynamics*, 31 (1) (1999) 1-22.
[11] A. Sackfield, D. Dini and D. A. Hills, Contact of a rotating wheel with a flat, *International Journal of Solids and Structures*, 44 (10) (2007) 3304-3316.
[12] A. Johansson and J. C. Nielsen, Out-of-round railway wheels—wheel-rail contact forces and track response derived from field tests and numerical simulations, *I. Mech. E, Part F: Journal of Rail and Rapid Transit*, 217 (2) (2003) 135-146.
[13] S. L. Grassie, R. W. Gregory, D. Harrison and K. L. Johnson, The dynamic response of railway track to high frequency vertical excitation, *Journal of Mechanical Engineering Science*, 24 (2) (1982) 77-90.
[14] J. Zhang, G. Han, X. Xiao, R. Wang, Y. Zhao and X. Jin, Influence of wheel polygonal wear on interior noise of high-speed trains, *Journal of Zhejiang University Science A*, 15 (12) (2014) 1002-1018.
[15] X. Wu, M. Chi and P. Wu, Influence of polygonal wear of railway wheels on the wheel set axle stress, *Vehicle System Dynamics*, 53 (11) (2015) 1535-1554.
[16] E. Brommundt, A simple mechanism for the polygonalization of railway wheels by wear, *Mechanics Research Communications*, 24 (4) (1995) 435-442.
[17] B. Morys, Enlargement of out-of-round wheel profiles on high speed trains, *Journal of Sound and Vibration*, 227 (5) (1998) 965-978.
[18] A. Johansson and C. Andersson, Out-of-round railway wheels—a study of wheel polygonalization through simulation of three-dimensional wheel – rail interaction and wear, *Vehicle System Dynamics*, 43 (8) (2005) 539-559.
[19] L. Ling, X. Xiao and X. Jin, Interaction of subway LIM vehicle with ballasted track in polygonal wheel wear development, *Acta Mechanica Sinica*, 27 (2) (2011) 297-307.
[20] X. Jin, L. Wu, J. Fang and L. Ling, An investigation into the mechanism of the polygonal wear of metro train wheels and its effect on the dynamic behaviour of a wheel/rail system, *Vehicle System Dynamics*, 50 (12) (2012) 1817-1834.
[21] X. Liu and W. Zhai, Analysis of vertical dynamic wheel/rail interaction caused by polygonal wheels on high-speed trains, *Wear*, 314 (1) (2014) 282-290.
[22] H. Claus and W. Schiehlen, Modeling and simulation of railway bogie structural vibrations, *Vehicle System Dynamics*, 29 (S1) (1998) 538-552.
[23] R. Schwertassek, O. Wallrapp and A. A. Shabana, Flexible multibody simulation and choice of shape functions, *Nonlinear Dynamics*, 20 (4) (1999) 361-380.
[24] Timoshenko, Method of analysis of statical and dynamical stresses in rail, *Proc. Second Int. Congress of Appl. Mech.*, Zurich (1926).
[25] X. Xiao, L. Ling and X. Jin, A study of the derailment mechanism of a high speed train due to an earthquake, *Vehicle System Dynamics*, 50 (3) (2012) 449-470.
[26] J. J. Kalker, A fast algorithm for the simplified theory of rolling contact, *Vehicle System Dynamics*, 11 (1) (1982) 1-13.
[27] J. J. Kalker, *Three-dimensional elastic bodies in rolling contact,* Springer Science & Business Media (1990).
[28] K. Arczewski and F. Czek, Friction models and stress recovery methods in vehicle dynamics modelling, *Multibody System Dynamics*, 14 (3) (2005) 205-224.
[29] *Standard B EN 13103: Railway applications-Wheelsets and bogies-Non-powered axles-Design method* (2001).
[30] N. F. Mechanics, *Fatigue crack growth analysis software*, Reference Manual Version (2008).

Xingwen Wu received his B.S. degree in manufacturing engineering from the Southwest Jiaotong University in 2010. He received his M.S. degree in vehicle engineering from Southwest Jiaotong University, State Key Laboratory of Traction Power, in 2012. He is currently a Ph.D. student in Southwest Jiaotong University, and an Academic Visitor in Concordia University, Montreal, Canada. His research interests include the vehicle dynamics, fatigue analysis for the components of railway vehicles.